Origin of Antimony Segregation in GaInSb/InAs Strained-Layer Superlattices

J. Steinshnider, J. Harper, and M. Weimer*
Department of Physics, Texas A&M University, College Station, Texas 77843

C.-H. Lin and S. S. Pei
Space Vacuum Epitaxy Center, University of Houston, Houston, Texas 77204

D. H. Chow
HRL Laboratories, LLC, Malibu, California 90265
(Received 1 June 2000)

We show how cross-sectional scanning tunneling microscopy may be used to reconstruct the Sb segregation profiles in GaInSb/InAs strained-layer superlattices. These profiles are accurately described by a one-dimensional model parametrizing the spatial evolution of an Sb seed at the InAs-on-GaInSb interface in terms of two-anion-layer exchange. We argue that the segregation seed, which decreases from $\frac{2}{3}$ to $\frac{1}{2}$ monolayer when growth conditions are made less anion rich, has its origin in the Sb-bilayer reconstruction maintained during GaInSb epitaxy.

PACS numbers: 68.35.Ct, 61.16.Ch, 68.55.Ln, 68.65.+g

Although cation segregation in III_A-V/III_B-V semiconductor heterostructures has been extensively studied [1–7], comparatively little is known concerning the reciprocal problem of anion segregation [8–10] during III-V_A/III-V_B epitaxy.

Segregation is an inherently asymmetric process that reflects a layer-by-layer competition, during growth, between strain- and/or bond-strength energies that favor expulsion of certain atoms to the surface and entropic factors that account for the tendency to nonetheless incorporate a fraction of these atoms in successively buried epitaxial layers. This competition, unless controlled [6], gives rise to spatially varying composition profiles in the vicinity of certain heterojunctions (e.g., AlAs-on-GaAs [7]), but not others (e.g., GaAs-on-AlAs [7]), that degrade interfacial abruptness and exert an undesirable influence on the optical [2,11,12] and transport [13] properties of III-V semiconductor superlattices and quantum wells. Antimony segregation, in particular, has been implicated as a contributor to the interfacial asymmetries noted in previous cross-sectional scanning tunneling microscopy (STM) [14–16] and x-ray photoelectron spectroscopy [8] studies of type-II GaSb/InAs and GaInSb/InAs heterojunctions, a suggestion only recently confirmed with desorption mass spectrometry [9,10].

Here we use cross-sectional STM to facilitate direct, atomic-scale measurements of the compositional grading in GaInSb/InAs superlattices caused by Sb segregation and show how such measurements lead to improved understanding of the role played by the GaInSb surface stoichiometry in initiating this phenomenon. Specifically, we describe new techniques for reconstructing the Sb segregation profiles in these (and related) structures from cross-sectional STM data that connect those profiles with monolayer roughness at the InAs-on-GaInSb interface. We next demonstrate that the profiles so constructed are accurately described within a one-dimensional model where segregation of an initial Sb seed, supplied by the GaInSb template, is promoted by way of sequential, two-anion-layer exchange during growth. We then show how the fits obtained with this model quantitatively constrain the seed to integer ratios interpretable as an equivalent Sb fraction in the terminating layer of the bilayer reconstruction maintained during GaInSb epitaxy and indicate how the observed dependence of the seed on growth conditions is consistent with a hierarchy of bilayer reconstructions containing progressively fewer Sb atoms per surface cell. Finally, we note that deliberate exploitation of this hierarchy may present a new opportunity for controlling Sb segregation in the GaInSb/InAs material system.

Two strained-layer superlattices—a 6.5/15.5 monolayer (ML) $GaIn_{0.25}Sb$/InAs structure fabricated at HRL Laboratories (SL_1) and a 6/14 ML $GaIn_{0.23}Sb$/InAs structure fabricated at the University of Houston (SL_2)—were evaluated for this study. The superlattice layers were deposited on (001)-oriented GaSb substrates at comparable temperatures, using cracked arsenic and antimony sources, together with a brief postgrowth anneal, in each case. These superlattice growths [17,18] likewise relied on nominally similar (1×3) GaInSb templates but used different molecular beam epitaxy (MBE) shutter sequences [19] to form an InAs-on-GaInSb interface. This common RHEED pattern notwithstanding, the V:III ratio during GaInSb epitaxy was less anion rich in one case ($\sim$1:1 for SL_1) than the other ($\sim$2.5:1 for SL_2). The completed structures were exposed in cross section by cleavage along a (110) or $(1\bar{1}0)$ plane in a separate ultrahigh vacuum STM chamber, and large-area surveys of

 0031-9007/00/85(21)/4562(4)$15.00 © 2000 The American Physical Society

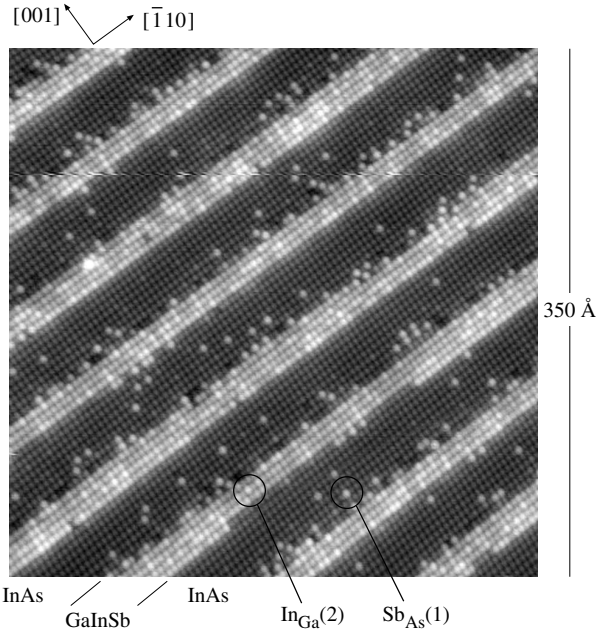

FIG. 1. Anion sublattice image of a GaInSb/InAs superlattice illustrating the characteristic antimony-for-arsenic and indium-for-gallium substitutional impurities in successive (110) planes. Growth direction is [001].

each set of superlattice layers assembled from overlapping atomic-resolution images.

Figure 1 shows a representative view of SL_1 in (110) cross section, where the bias polarity was chosen to image the filled-state density associated with As and Sb [20]. Isolated bright sites in the GaInSb layers point to the *controlled* isovalent substitution of In for Ga—in the (110) plane directly beneath the cleavage surface—during growth of the ternary alloy [4]. This localized signature is a predominantly geometric effect, arising from the replacement of a GaSb-like back bond with a longer InSb-like one [21]. Isolated bright sites in the InAs layers point to the *uncontrolled* isovalent substitution of Sb for As—in the cleavage plane itself—following segregation and cross incorporation [22]. The localized bright appearance, here, is due to an InSb-like back bond as well as the replacement of an As dangling bond with an Sb one [23].

It is clear following examination of Fig. 1 that the antimony-for-arsenic substitutional fraction is noticeably greater in As rows nearer the InAs-on-GaInSb heterojunction than in those farther away. This asymmetric, compositional grading in the [001] direction is qualitatively consistent with Sb segregation during growth and, as we now show, accurately described by a one-dimensional segregation model [24].

Adopting the notation of Muraki *et al.* [2], we presume that the growth template (GaInSb) provides a segregation seed (Sb), represented by an initial impurity fraction x_i, and that, following exposure to an incoming flux of nonsegregating material (InAs), a fraction R of this seed—where R defines a phenomenological segregation coefficient—is expelled to the surface as a floating layer and the remainder, $1 - R$, incorporated into a newly completed anion monolayer (As). This partitioning between a floating layer and each progressively buried anion layer is repeated until the available seed is exhausted or the process interrupted with growth of a new material (GaInSb). The ensuing segregation profile is then defined through the homogeneous recursion relations

$$x_{\text{floating}}(n) = R[x_{\text{floating}}(n - 1)],$$
$$x(n) = (1 - R)[x_{\text{floating}}(n - 1)],$$

subject to the initial condition $x_{\text{floating}}(0) = x_i$, with n an integer label indexing successively buried anion planes and $x(n)$ the incorporated impurity fraction in each.

If, as often occurs during mixed-anion epitaxy, there is an unwanted vapor background that promotes the cross incorporation of segregating atoms, one must also account for the contribution from this process to the impurity fraction in each layer. The segregation profile independently generated by cross incorporation is defined through the inhomogeneous recursion relations

$$x_{\text{floating}}(n) = R[x_{\text{floating}}(n - 1) + x_0],$$
$$x(n) = (1 - R)[x_{\text{floating}}(n - 1) + x_0],$$

subject to the initial condition $x_{\text{floating}}(0) = 0$, with x_0 a constant source term from the vapor. Combining the solutions to these two, independent sets of recursion relations yields

$$x(n) = x_i R^{n-1}(1 - R) + x_0(1 - R^n) \qquad (1)$$

for the final impurity profile. Particularizing to the situation in Fig. 1, the first term represents a geometric (i.e., exponential) falloff in the Sb fraction in successive As layers whose sum is the initial seed (x_i) at the InAs-on-GaInSb interface, whereas the second accounts for a nonzero, asymptotic Sb fraction (x_0) due to background incorporation.

Calculation of an empirical Sb fraction for each cleavage-exposed As row is a straightforward matter of normalizing the number of antimony-for-arsenic substitutions observed to the number of As sites sampled with STM images such as the one in Fig. 1. What is *not* straightforward is the mapping of these rows onto the (001) planes in Eq. (1). The difficulty is illustrated in Fig. 2 (top), where we show the InAs-on-GaInSb heterojunction in [1$\bar{1}$0] perspective following one of two conceivable (110) cleaves. The As dangling bonds created during this cleave occur in *every other* (001) plane so that only half these planes—in this case, the n-even subset—are visible with STM; were the cleavage surface to shift a monolayer in the [110] direction, a complementary subset—in this case, the n-odd planes—would be exposed. Related complications occur at [001] kinks along the InAs-on-GaInSb heterojunction arising from monolayer roughness in the growth plane. As illustrated in Fig. 2,

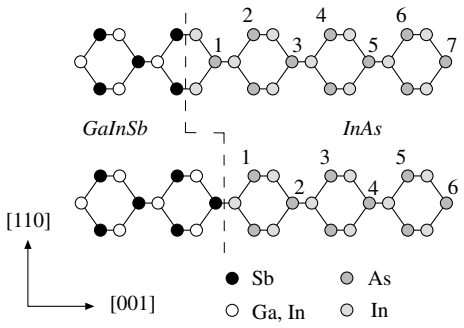

FIG. 2. (Top) Schematic InAs-on-GaInSb heterojunction in $[1\bar{1}0]$ perspective. Cleavage across a kink-free segment of the interface exposes an even (or odd) subset of (001) As planes. (Bottom) Monolayer roughness transforms this subset from even to odd (or vice versa).

these kinks transform an even sequence of cleavage-exposed As planes into an odd one, and vice versa.

We now demonstrate how both difficulties may be circumvented — and the *complete* segregation profile quantitatively reconstructed from an appropriate ensemble of cross-sectional STM data — under suitable conditions. We approach this task by observing that the two subsets of As planes, are, in principle, distinguished by different mean Sb fractions per exposed layer, $\langle x(n)\rangle_n$; odd sequences, being, on average, 1 ML closer to the InAs-on-GaInSb interface than even ones, should exhibit higher Sb content. That distinction will be obscured to the extent interface wandering mixes even and odd sequences together, suggesting an important relationship between the lateral length scales employed to perform our impurity counting and those that characterize monolayer roughness. For example, were we to perform the counting over long stretches of an InAs-on-GaInSb heterojunction that adopted each of the configurations in Fig. 2 with equal probability, these two, otherwise distinct Sb populations would obviously coalesce.

Figure 3 displays a frequency histogram of the mean Sb fractions observed in 25 independent samplings of the InAs wells throughout a geometrically contiguous region of SL_1 encompassing several repeats. These samplings comprised the first six, cleavage-exposed As planes above selected, 100 to 300 lattice-site-long segments of the InAs-on-GaInSb interface free of visible kinks. The histogram clearly suggests two populations. This hypothesis is confirmed, and the parameters governing the respective parent distributions accurately estimated, with a hierarchical cluster analysis [25] that systematically partitions our observations into distinct $\langle x(n)\rangle_n$ populations without the (arbitrary) binning required to form a histogram. The Gaussian parent distributions deduced from this analysis are likewise shown in Fig. 3.

Adopting the cluster partitioning of these observations into high and low Sb-fraction groups, we then average $x(n)$, for fixed n, over the appropriate *subensemble* (even or odd) to obtain the points assembled into the segregation profiles illustrated in Fig. 4. The interleaving data from SL_1 and SL_2 form single, continuous curves that are each accurately described by Eq. (1). The self-consistency of the cluster partitioning for SL_1 is demonstrated in Fig. 3, where dashed lines mark the mean Sb fractions $\langle x(n)\rangle_n$, predicted from (1) with the fit parameters listed in Table I.

The smooth decay of the segregation profiles in Fig. 4 argues that our discrimination between high and low Sb-fraction groups is maximal. Thus, from the standpoint of *anion segregation,* the InAs-on-GaInSb interface appears planar and abrupt over length scales of 400–1000 Å. This conclusion is confirmed with fits to a generalization of (1) where even and odd sequences are weighted with the respective probabilities for adopting each of the configurations shown in Fig. 2; such fits yield a "segregation roughness" statistically indistinguishable from zero.

Although the segregation coefficients for SL_1 and SL_2 are comparable (Table I), their Sb seeds are clearly different. These seeds are close to integer ratios — $\frac{1}{2}$ and $\frac{2}{3}$, respectively — whose values afford direct interpretation. Consider the $x_i = \frac{2}{3}$ result first. The (1×3) reconstruction of GaInSb is usually thought terminated with an extra $\frac{2}{3}$ ML of Sb — Sb dimers [26–28] atop a complete Sb monolayer back bonded to metal atoms (Fig. 5). It is quite natural, from the standpoint of such a stoichiometry, to suppose this *additional* $\frac{2}{3}$ ML *is* the initial Sb seed. That

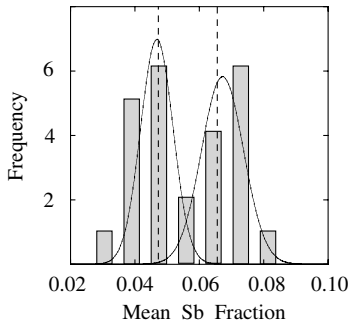

FIG. 3. Frequency histogram of the cleavage-exposed Sb fraction in SL_1. Smooth curves are the parent distributions from cluster analysis, dashed lines the cluster means predicted with the fit in Fig. 4.

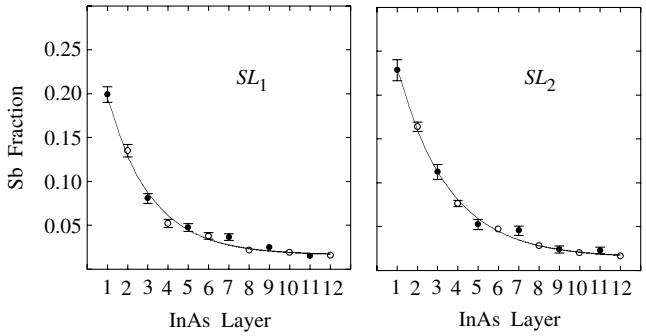

FIG. 4. Segregation profiles constructed from interleaving even (open symbols) and odd (closed symbols) samplings of the As planes in SL_1 (left) and SL_2 (right). Solid lines are fits to Eq. (1).

TABLE I. Summary of segregation model fit parameters.

	SL_1	SL_2
x_i	0.51 ± 0.02	0.69 ± 0.02
R	0.63 ± 0.02	0.67 ± 0.01
x_0	0.016 ± 0.002	0.015 ± 0.002

suggestion also makes sense in terms of bond energetics: because an Sb—Sb bond is considerably weaker than either an In—Sb or Ga—Sb one [29], there is a ready preference for these less tightly bound Sb atoms to be expelled and form a floating layer; since an In—As bond is stronger than an In—Sb one, similar logic rationalizes the maintenance of this floating layer above an evolving InAs film.

The same paradigm calls for fewer top-layer Sb atoms per surface cell to explain a $x_i = \frac{1}{2}$ result. We therefore contend that SL_1 and SL_2 possess distinct bilayer surface reconstructions—consistent with the less anion-rich growth conditions employed for SL_1—whose excess Sb stoichiometries are $\frac{1}{2}$ and $\frac{2}{3}$ ML, respectively. These reconstructions, illustrated schematically in Fig. 5, are intrinsically (4×3)-like and similar to ones recently observed with *in situ* STM [30] on quenched AlSb and GaSb (001) surfaces when the antimony flux during growth is varied.

It is worth noting that the structures shown in Fig. 5 are drawn from a sequence of (4×3) surface cells whose excess Sb stoichiometries systematically decrease, in $\frac{1}{12}$ ML steps, from $\frac{2}{3}$ to $\frac{1}{3}$ ML as top-layer Sb—Sb dimers are progressively replaced with Sb—Ga(In) ones to satisfy electron counting requirements [30]. Thus, our argument that MBE growth conditions directly influence the Sb seed through their effect on the bilayer reconstruction suggests deliberate exploitation of this sequence may offer a new and potentially promising avenue for the control of Sb segregation in GaInSb/InAs superlattices and related arsenide-antimonide heterostructures.

In conclusion, we have used cross-sectional STM to facilitate direct, atomic-scale measurements of the compositional grading at InAs-on-GaInSb heterojunctions caused by Sb segregation and shown how these composition profiles are quantitatively linked with the anion stoichiometry of the GaInSb surface reconstructions that serve as the templates for interface formation.

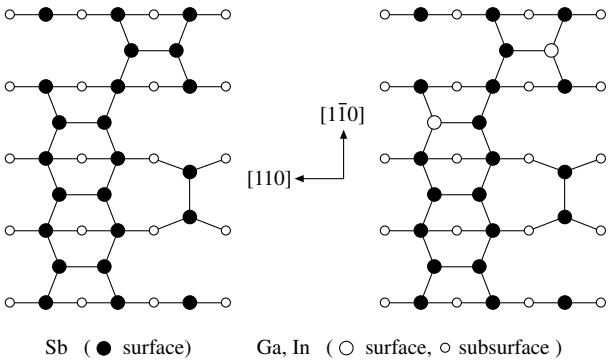

FIG. 5. Schematic GaInSb (001) surface reconstructions compatible with Sb segregation seeds of $\frac{2}{3}$ (left) and $\frac{1}{2}$ (right) ML, respectively.

The authors are indebted to M. Speed for acquainting them with hierarchical cluster analysis. This work was supported by the National Science Foundation (DMR-9633011) and Air Force Research Laboratory.

*Electronic address: weimer@tamu.edu

[1] J. M. Moison *et al.,* Phys. Rev. B **40**, 6149 (1989).
[2] K. Muraki *et al.,* Appl. Phys. Lett. **61**, 557 (1992).
[3] J. F. Zheng *et al.,* Phys. Rev. Lett. **72**, 2414 (1994).
[4] M. Pfister *et al.,* Appl. Phys. Lett. **67**, 1459 (1995).
[5] G. S. Spencer *et al.,* Phys. Rev. B **52**, 8205 (1995).
[6] R. Kaspi and K. R. Evans, Appl. Phys. Lett. **67**, 819 (1995).
[7] W. Braun *et al.,* Phys. Rev. B **55**, 1689 (1997).
[8] M. W. Wang *et al.,* J. Vac. Sci. Technol. B **13**, 1689 (1995).
[9] R. Kaspi and K. R. Evans, J. Cryst. Growth **175/176**, 838 (1997).
[10] R. Kaspi, J. Cryst. Growth **201/202**, 864 (1999).
[11] P. M. Young and H. Ehrenreich, Appl. Phys. Lett. **61**, 1069 (1992).
[12] B. Koiller, R. B. Capaz, and H. Chacham, Phys. Rev. B **60**, 1787 (1999).
[13] M. J. Shaw, Phys. Rev. B **61**, 5431 (2000).
[14] R. M. Feenstra *et al.,* Phys. Rev. Lett. **72**, 2749 (1994).
[15] R. M. Feenstra *et al.,* J. Vac. Sci. Technol. B **12**, 2592 (1994).
[16] A. Y. Lew *et al.,* Appl. Phys. Lett. **70**, 75 (1997).
[17] R. H. Miles *et al.,* Appl. Phys. Lett. **66**, 1921 (1995).
[18] C.-H. Lin *et al.,* Proc. SPIE Int. Soc. Opt. Eng. **3628**, 22 (1998).
[19] The principal distinction was a 3-sec antimony soak for SL_1 versus a 4-sec total growth interrupt for SL_2; see [17,18].
[20] The contrast between InAs and GaInSb is an electronic effect; see [15].
[21] Replacement of an InAs-like back bond by a shorter GaAs-like one conversely accounts for the occasional dark sites at the InAs-on-GaInSb interfaces in Fig. 1; see, for example, J. Steinshnider *et al.,* Phys. Rev. Lett. **85**, 2953 (2000).
[22] R. M. Feenstra, D. A. Collins, and T. C. McGill, Superlattices Microstruct. **15**, 215 (1994).
[23] J. Harper *et al.,* Appl. Phys. Lett. **73**, 2805 (1998).
[24] There is a long history to such models. See, for example, [1], and references therein.
[25] R. A. Johnson and D. W. Wichern, *Applied Multivariate Statistical Analysis* (Prentice Hall, Upper Saddle River, NJ, 1998), 4th ed.
[26] C. F. McConville *et al.,* Phys. Rev. B **50**, 14 965 (1994).
[27] M. T. Sieger, T. Miller, and T.-C. Chiang, Phys. Rev. B **52**, 8256 (1995).
[28] U. Resch-Esser *et al.,* Phys. Rev. B **55**, 15 401 (1997).
[29] I. Barin, *Thermochemical Data of Pure Substances* (VCH, Weinheim, 1989).
[30] W. Barvosa-Carter *et al.,* Phys. Rev. Lett. **84**, 4649 (2000).